Coverage dependent adsorption dynamics in hyperthermal organic thin film growth

A. Amassian,[1] T. V. Desai,[2] S. Kowarik,[2,3] S. Hong,[2] A. R. Woll,[4] G. G. Malliaras,[1] F. Schreiber,[3] and J. R. Engstrom[2,a)]

[1]*Department of Materials Science and Engineering, Cornell University, Ithaca, New York 14853, USA*
[2]*School of Chemical and Biomolecular Engineering, Cornell University, Ithaca, New York 14853, USA*
[3]*Institute für Angewandte Physik, Universität Tübingen, 72076 Tübingen, Germany*
[4]*Cornell High Energy Synchrotron Source, Cornell University, Ithaca, New York 14853, USA*

We have examined the dynamics of adsorption of diindenoperylene (DIP) on SiO_2 and SiO_2 modified with an interfacial organic layer using *in situ* real time synchrotron x-ray scattering, focusing on the effects of coverage. On both surfaces we observe a substantial increase in the probability of adsorption with increasing coverage, which is most dramatic at the highest incident kinetic energies. On the initially uncovered surfaces, we observe a smooth decrease in the probability of adsorption with increasing incident kinetic energy, indicative of trapping-mediated adsorption. Once both surfaces are covered by DIP, the effects of incident kinetic energy are greatly reduced, and trapping is very efficient over the range of kinetic energies examined. Possible reasons for efficient trapping at high coverage and at high incident kinetic energy include more efficient momentum transfer due to mass matching, and possibly direct molecular insertion. Comparison to results on another small-molecule, pentacene, suggests that this behavior should be common to hyperthermal growth of a variety of other small-molecule thin films. © *2009 American Institute of Physics.* [DOI: 10.1063/1.3088835]

I. INTRODUCTION

Conjugated small molecules have garnered significant attention in recent years owing to their ability to assemble into highly ordered semiconductors with electronic transport characteristics surpassing those of amorphous Si,[1,2] currently the material of choice for manufacturing thin film transistors (TFTs). The molecular packing structure, the efficiency of π-π^* coupling, the number of grain boundaries in polycrystalline organic semiconductor films, and interfacial trap states essentially mediate charge transport in organic TFTs.[3,4] The realization that the performance of these devices is intimately linked to the molecular packing, microstructure, and morphology of the organic semiconductor and to the surface chemistry of the gate dielectric has led to studies of the mechanisms of growth and ordering of conjugated small-molecular building blocks on inorganic substrates.[5–9] This has also spurred efforts to influence the growth behavior by modifying the substrate surface chemically[10,11] or physically.[12]

Typically, small-molecule thin films are deposited by vacuum sublimation or evaporation processes. The simplicity of these thermal processes makes them attractive, but they lack versatility to tailor the growth of molecular films as growth rate (GR) and substrate temperature are essentially the only process parameters. Alternative methods are available[13–15] which offer additional process parameters to possibly manipulate the growth behavior of thin films.

Among these, supersonic molecular beams stand out because of their ability to tune the state of incident molecules in the vapor phase, including their translational kinetic energy,[16–22] angle of incidence,[18] and their state of aggregation, e.g., via formation of van der Waals clusters.[23,24]

The kinetic energy of the incident molecular flux is expected to affect most directly the probability of molecular adsorption, i.e., the trapping probability, as this energy must be dissipated in some way to bind the molecule to the surface. The dynamics of adsorption of relatively simple molecules on typically inorganic substrates (e.g., transition metals) has been extensively studied.[25] Study of more complex molecules, and the examination of more complex surfaces such as those provided by liquids[26] and surfaces terminated with self-assembled monolayers[27] is much less wide spread. Concerning organic thin film growth, increasing the incident kinetic energy has been shown to decrease the trapping probability of pentacene on SiO_2 substrates, while the dependence on the angle of incidence follows neither normal nor total energy scaling.[18] The effect of incident kinetic energy in the multilayer regime, particularly the evolution of surface roughness of pentacene thin films, is currently a matter of discussion, as we have not found any significant changes in the growth mode with incident kinetic energy from *in situ* real time synchrotron x-ray scattering and *ex situ* atomic force microscopy (AFM).[22] Moreover, from molecular dynamics simulations[28] and experiments[29] by our group we find that, at least for pentacene on SiO_2 surfaces, there are important contributions of events such as direct molecular insertion of pentacene into previously existing pentacene layers at sufficiently high incident kinetic energies, and these are
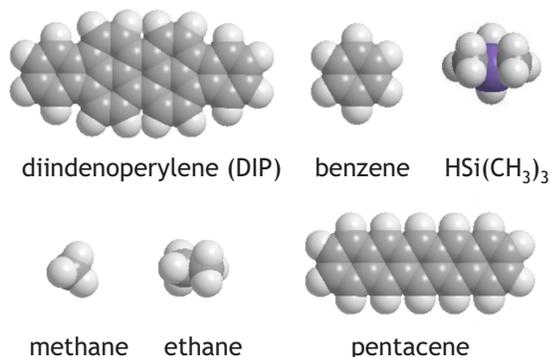
FIG. 1. (Color online) Space filling models for the primary molecule of interest here, DIP, and two related acenes, pentacene, and benzene. We also show two molecules more commonly studied in the field of gas-surface dynamics, methane, and ethane, and the chemisorbing species formed upon exposure of SiO_2 to HMDS, $HSi(CH_3)_3$, where H represents the SiO_2 surface.

manifest in an increase in the trapping probability with increasing coverage.

In order to determine how universal the changes are with increasing coverage in the kinetics of growth of organic thin films from hyperthermal sources we examine here the growth of diindenoperylene (DIP) on clean SiO_2 and SiO_2 modified with an interfacial organic layer, hexamethyldisilazane, $HN[Si(CH_3)_3]_2$, HMDS. Space filling models for DIP and pentacene are shown in Fig. 1. DIP is known to grow in a more sustained layer-by-layer mode than pentacene on SiO_2,[30] which will allow us to make use of *in situ* real time synchrotron x-ray scattering to monitor the growth from the submonolayer regime to that corresponding to the formation of several layers. Such experiments were not possible with pentacene, as the films roughen quickly, dampening the intensity at the anti-Bragg condition $(00\frac{1}{2})$.[22] For DIP we are able to measure the rate of growth for the first few layers using x-ray scattering and we find that the rate of adsorption changes significantly as the coverage of adsorbed molecules increases, and that the relative amount of increase depends on the incident kinetic energy. We discuss the possible molecular scale events that may lead to this acceleration in the rate of growth.

II. EXPERIMENTAL PROCEDURES

The experiments were carried out in the G3 station of the Cornell High Energy Synchrotron Source in a custom-designed ultrahigh vacuum chamber fitted with Be windows that is described in detail elsewhere.[31] Briefly, the system consists of four separately pumped chambers: a main scattering chamber; a source chamber, where the supersonic nozzle resides; an antechamber separating the source and main chambers, which houses a beam shutter and rotating blade chopper; and a fast entry load lock. All chambers are pumped by high-throughput turbomolecular pumps. The base pressure of the chamber was typically $\sim 4 \times 10^{-9}$ Torr and samples were loaded via the load-lock chamber, which was evacuated to $\sim 10^{-7}$ Torr prior to sample transfer into the main chamber.

Substrates were 4 in. Si (100) wafers (Wacker-Siltronic, *p*-type, 500–550 μm thick, 38–63 Ω cm) subject to an SC-1 clean, 15 s HF dip and SC-2 clean immediately before growth of SiO_2. Approximately 300-nm-thick SiO_2 films were grown by wet thermal oxidation at 1100 °C. HMDS was deposited on a number of these samples from the vapor phase using a YES LP-III Vapor Prime Oven after successive evacuation and purge cycles to dehydrate the substrate held at 150 °C. Immediately prior to placement into the load lock of the vacuum chamber, bare oxide wafers were cleaned and degreased by sonication for 15 min in anhydrous $CHCl_3$ solution (99%+), sonicated in H_2O for 15 min, washed with de-ionized (DI) water, dried with N_2, and subjected to UV-ozone cleaning for 15 min.

Supersonic molecular beams of DIP were generated by passing a carrier gas (He, 99.999% Air Gas Inc.) over a temperature controlled container (the evaporator) located upstream of the nozzle in the source chamber. The flow of carrier gases was modulated using a mass flow controller (MKS). The nozzle (heatable) consisted of 0.25 in. diameter stainless steel tubing, with a 125 μm thick plate of stainless steel welded at its end. This plate had a 150 μm orifice machined into it. The doubly differentially pumped beam passed through a trumpet shaped skimmer (1.5 mm aperture, Beam Dynamics Inc.) into an antechamber and through a large aperture that produced a well-defined rectangular beam spot (4×15 mm^2) on the substrate at normal incidence. Using He as a carrier gas, the energy of the beam of DIP could be varied from 5.1 to 12.3 eV as determined from time of flight measurements.[31] The flux of DIP was varied by adjusting the temperature of the evaporator (typically, $T_b \sim 320$ °C). In all cases the beam was incident normal to the substrate surface, and could be blocked using a shutter in the antechamber, facilitating precise exposures of the substrate to the molecular beam. Multiple experiments could be carried out on the same substrate, which is made possible by translating the substrate perpendicular to the supersonic molecular beam, and due to the high beam-to-background flux ratio. During deposition the substrate temperature was kept at $T_s = 64$ °C. The GR of DIP ranged between 0.0019 and 0.0086 ML s^{-1} (ML denotes monolayer) for the submonolayer regime, and 0.0068 and 0.013 ML s^{-1} for the multilayer regime. Following deposition, atomic force microscopy was conducted *ex situ* in tapping mode using a DI 3100 Dimension microscope.

Growth of DIP was monitored *in situ* and in real time by x-ray synchrotron scattering, using 9.75 keV x rays incident at an angle of 1.11° (with respect to the substrate surface) with a flux of $\sim 10^{13}$ photons s^{-1}, incident to the sample through a Be window with energy resolution of 1% dictated by the use of a multilayer monochromator. A Bede scintillator counter was used for measuring the scattered x-ray intensity. Both static $(0 < q_z < 1.0$ Å$^{-1})$ and time-resolved anti-Bragg $(00\frac{1}{2}; q_z = q_{\text{Bragg}}/2 = 0.37/2$ Å$^{-1})$ x-ray reflectivity measurements were performed. The latter is an effective monitor of the nature of growth, i.e., layer-by-layer (LbL) versus three dimensional (3D) islanded growth.

The anti-Bragg x-ray data were fitted using a modified

version[32] of the mean-field, rate equation model of growth first proposed by Cohen *et al.*[33] The equations for the coverage of individual layers (θ_n) are given by

$$\frac{d\theta_n}{dt} = S_{n-1}F[(\theta_{n-1} - \theta_n) - \alpha_{n-1}(\theta_{n-1} - \theta_n)]$$

$$+ S_n F \alpha_n (\theta_n - \theta_{n+1}), \tag{1}$$

where $n=0$ represents the substrate, $n=1$ the first molecular layer, etc., S_n is the probability of adsorption for molecules incident on the nth layer, F is the incident molecular flux (ML s^{-1}), and α_n is the fraction of molecules that initially impact and land on top of the nth layer, but rather than staying on the top of that layer, drop down and become part of that layer via some mechanism. The latter includes "downward" interlayer transport of molecules across a step edge, but also includes events such as direct molecular insertion. In this solid-on-solid model $\theta_{n-1} > \theta_n$. In the absence of adsorption of molecules on themselves, Eq. (1) reduces to $d\theta_1/dt = S_0 F(1 - \theta_1)$, the rate expression expected for simple molecular adsorption on a surface. Here we will assume that there are two values for the probability of adsorption: one for adsorption on the substrate (S_0), and one for that on previously existing molecular layers, independent of their thickness ($S_1 = S_2 = S_3, \ldots$). Concerning interlayer transport we will assume that three values are possible (note, as the substrate cannot be penetrated, $\alpha_0 = 0$), namely, α_1, α_2 and $\alpha_{n \geq 3}$. There is also a coverage dependence built into these interlayer transport coefficients, which is described in detail elsewhere.[32,33] Finally, "upward" interlayer transport (movement from the n to the $n+1$ layer) is not factored into this model.

Once layer coverages have been calculated by integrating Eq. (1), these can then be used to calculate the x-ray intensity as a function of time.[9,22,32–35] The intensity of the scattered beam (I) depends upon the layer population according to the following relationship:

$$I(t) = \left| r_{subs} e^{-i\phi} + r_{film} \sum_{n=1}^{\infty} \theta_n(t) e^{-iq_z dn} \right|^2, \tag{2}$$

where r_{subs} and r_{film} are the reflection amplitudes of the substrate and the film, ϕ is the phase change upon reflection, q_z is the out-of-plane scattering vector, and d is the out-of-plane interplanar spacing. At the so-called anti-Bragg position, $q_z d = \pi$, which results in a change in the sign of the thin film terms in the summation with the filling of each successive layer.

III. RESULTS AND DISCUSSION

In Figs. 2–5 we present a subset of experiments we have conducted concerning the growth of DIP on clean SiO$_2$, and SiO$_2$ that has been modified with HMDS. The data shown represent the lowest (5.1 eV) and highest (12.3 eV) kinetic energies examined here using the supersonic molecular beam source. All experiments were conducted at $T_s = 64$ °C. In Fig. 2(a) we present the scattered x-ray intensity acquired in real time at the anti-Bragg condition ($q_z = 00\frac{1}{2}$) for the growth of DIP on SiO$_2$ at $E_i = 5.1$ eV. As suggested in connection with
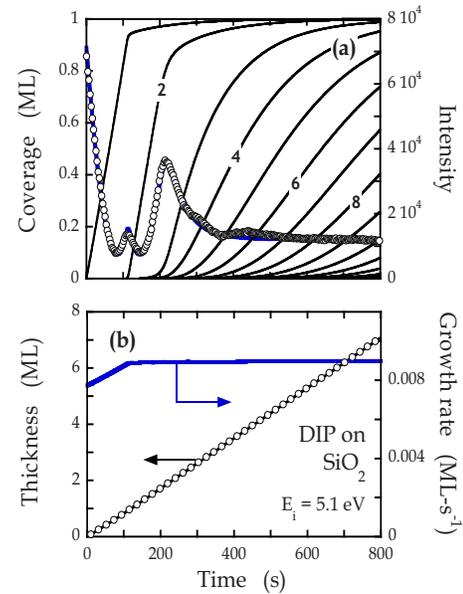
FIG. 2. (Color online) (a) X-ray intensity at the anti-Bragg condition as a function of exposure to the molecular beam ($E_i = 5.1$ eV) for thin films of DIP deposited on clean SiO$_2$. $T_s = 64$ °C. Thick solid lines (right ordinate) indicate a fit of the data to a model and thin solid curves (left ordinate) represent predicted coverages (θ_n) of the individual layers. (b) Total coverage (θ_{tot}, left ordinate) and GR (right ordinate) predicted by a fit of the data displayed in (a).

Eq. (2), intensity oscillations for this scattering condition are expected due to alternating contributions of the odd and even layers to the magnitude of the scattered intensity. Depending upon the reflection amplitudes (r_{subs} and r_{film}) and the phase change (ϕ), thin film growth can lead to either one or two maxima for every 2 ML of growth. As may be seen in Fig.
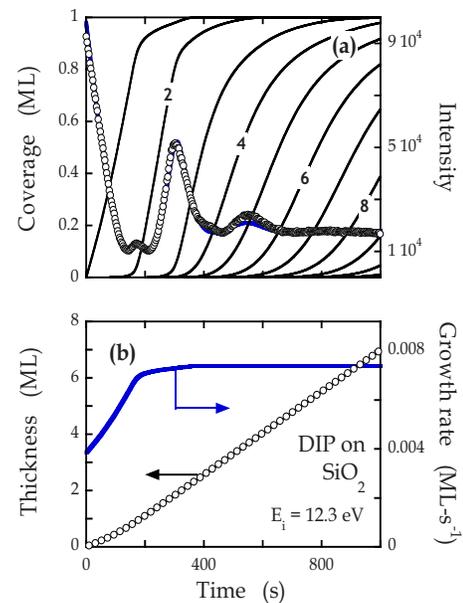
FIG. 3. (Color online) (a) X-ray intensity at the anti-Bragg condition as a function of exposure to the molecular beam ($E_i = 12.3$ eV) for thin films of DIP deposited on clean SiO$_2$. $T_s = 64$ °C. Thick solid lines (right ordinate) indicate a fit of the data to a model and thin solid curves (left ordinate) represent predicted coverages (θ_n) of the individual layers. (b) Total coverage (θ_{tot}, left ordinate) and GR (right ordinate) predicted by a fit of the data displayed in (a).
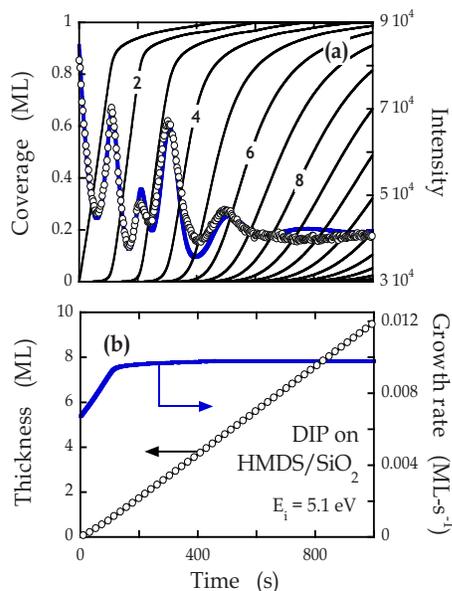
FIG. 4. (Color online) (a) X-ray intensity at the anti-Bragg condition as a function of exposure to the molecular beam (E_i=5.1 eV) for thin films of DIP deposited on SiO_2 modified with HMDS. T_s=64 °C. Thick solid lines (right ordinate) indicate a fit of the data to a model and thin solid curves (left ordinate) represent predicted coverages (θ_n) of the individual layers. (b) Total coverage (θ_{tot}, left ordinate) and GR (right ordinate) predicted by a fit of the data displayed in (a).

2(a) for these conditions we see a small maximum, followed by a much larger one. The second pair of small and larger maxima are almost entirely obscured, however, after which the intensity oscillations have become strongly damped, indicating 3D growth. Approximately, these maxima correspond to deposition of 1, 2, 3, and 4 ML of DIP on SiO_2.
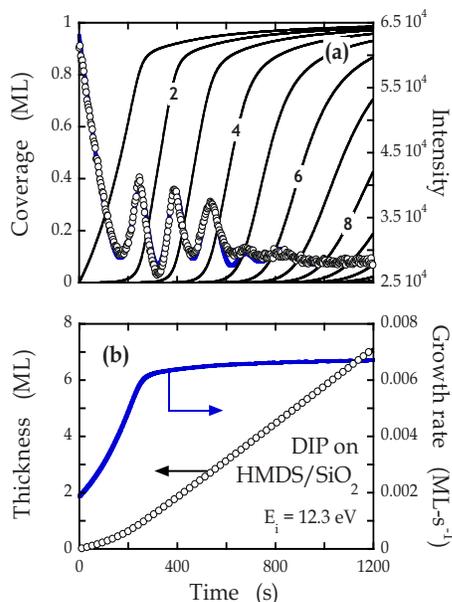
FIG. 5. (Color online) (a) X-ray intensity at the anti-Bragg condition as a function of exposure to the molecular beam (E_i=5.1 eV) for thin films of DIP deposited on SiO_2 modified with HMDS. T_s=64 °C. Thick solid lines (right ordinate) indicate a fit of the data to a model and thin solid curves (left ordinate) represent predicted coverages (θ_n) of the individual layers. (b) Total coverage (θ_{tot}, left ordinate) and GR (right ordinate) predicted by a fit of the data displayed in (a).

The kinetics of growth can be modeled more precisely by making use of both Eqs. (1) and (2) and these results are shown in Figs. 2(a) and 2(b). In (a) we show the coverage (occupancy) of each layer predicted by the fit to the intensity oscillations as shown by the solid blue line. Most important to the discussion here, we find that to fit the data we need to assume that $S_0 F \sim 0.0077$ ML s^{-1}, whereas $S_{n \geq 1} F \sim 0.0090$ ML s^{-1}. Thus, these data indicate that the rate of growth has accelerated with increasing thickness/coverage. Since adsorption is essentially irreversible for these conditions (desorption is negligible) these data indicate that the acceleration in the rate is due to an increase in the adsorption probability S with increasing coverage. In this case the adsorption probability has increased by about 16%.

We consider additional results in Fig. 3, where here DIP is incident on SiO_2 at E_i=12.3 eV. Comparing these results to those shown in Fig. 2 we notice two important differences. First, the second of the larger maxima (corresponding to ~4 ML of DIP) is more pronounced for these conditions, indicating that LbL growth is more extended for these conditions. Second, the difference between the initial rate of growth, and that achieved at longer times and higher coverages is now much different—to fit these data we must assume that $S_0 F \sim 0.0039$ ML s^{-1}, whereas $S_{n \geq 1} F \sim 0.0074$ ML s^{-1}, an increase of nearly 90%. If we consider intermediate kinetic energies we find results for this acceleration in the rate of growth that are intermediate between those shown in Figs. 2 and 3, and they exhibit a consistent trend with E_i, namely a 49% increase at E_i=7.7 eV, and 64% at E_i=10.9 eV.

In Figs. 4 and 5 we display the results for the growth of DIP on SiO_2 modified with HMDS. As may be seen the intensity oscillations show both similarities and differences between those for growth on SiO_2. Again we see maxima for approximately the completion of each monolayer, but for growth on the HMDS-modified surface the intensities associated with the completion of the first and third monolayers are approximately equal or exceed that for growth on the second and fourth monolayers, which differs from that on clean SiO_2. This is simply due to changes in the reflection amplitude(s) and the phase change produced by the thin interfacial organic layer. At the lowest kinetic energy (5.1 eV) from Fig. 4 we see that the intensity oscillations for approximately the first 4 ML are more pronounced than those observed for growth on clean SiO_2 at the same energy. This suggests that LbL growth is more extended on the HMDS-modified surface for these conditions. From Fig. 4(b) we see that on this surface a change in the rate of growth (bare substrate versus multilayer) is also observed, and for this energy the amount of increase is ~46%, a value larger than the amount of acceleration observed on clean SiO_2 at this same E_i. At the highest kinetic energy (12.3 eV), in Fig. 5 we see that the intensity of the oscillations appear to be somewhat more damped at the higher energy, suggesting somewhat rougher growth at the higher energy. Concerning the kinetics of growth, acceleration in the rate of growth at the highest energy is clearly evident on the HMDS-modified surface, and the increase in this case is about 262%. Again, for the two intermediate cases we do not display here, we find
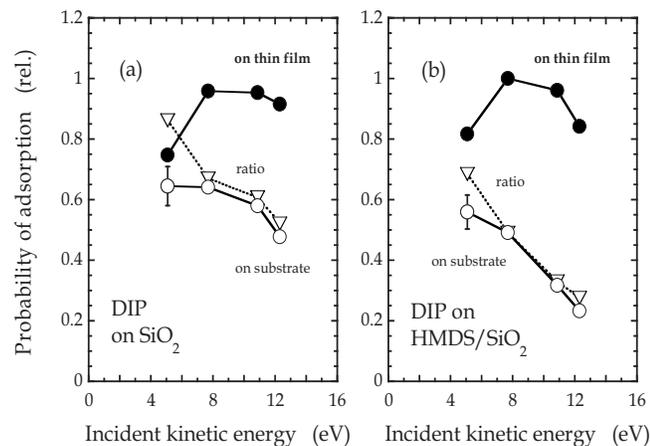
FIG. 6. Relative probabilities of adsorption of DIP on (a) clean SiO_2; and on (b) SiO_2 modified with HMDS. Results are shown for DIP on the bare substrates and DIP on the growing DIP thin film. All data have been normalized to the highest GR observed here (growth in the multilayer regime on HMDS-modified SiO_2 at $E_i=7.7$ eV), and corrected for differences in the incident flux. The ratio of the two probabilities is also shown for each case (triangles). A representative error bar ($\pm 10\%$) is shown in each panel.

results that are intermediate and that establish a trend concerning the amount of acceleration: an approximately 104% increase at $E_i=7.7$ eV and $\sim 203\%$ at $E_i=10.9$ eV.

It should be clear that our results show conclusively that—for the systems we have examined here—the probability of adsorption differs significantly for adsorption in the submonolayer and multilayer regimes, and that this difference becomes larger with increasing energy. Unfortunately, we measure only the product SF directly, and measurement of the absolute incident flux using standard methods is not feasible. We can, however, use quadrupole mass spectrometry (QMS) to measure the relative incident molecular flux, after correcting for the velocity of the DIP molecules. We have done so making use of a QMS placed in the direct path of the beam in experiments separate from those displayed in Figs. 2–5. Thus these results (run to run) may be affected by the reproducibility of the flux produced by the supersonic beam, and we estimate this uncertainty to be about $\pm 5\%$, not exceeding $\pm 10\%$. The change in incident flux during the course of an experiment and its impact on comparing submonolayer to multilayer GRs, on the other hand, is closer to $\pm 1\%$. These facts should be kept in mind in the discussion to follow.

In Fig. 6 we present the relative probabilities of adsorption as a function of the incident kinetic energy after making an appropriate accounting for the change in the incident flux for the beams representing different E_i's. We have normalized these results for the highest flux-corrected GR we observe here, namely, growth on HMDS-modified SiO_2 at $E_i=7.7$ eV. In Fig. 6(a) we plot results for the adsorption of DIP on SiO_2, and in (b) for DIP on HMDS-modified SiO_2. In both cases we plot both the clean substrate (S_0) and the thin film covered substrate ($S_{n\geq 1}$) probabilities of adsorption. On both surfaces the probability of adsorption at high coverage exhibits little dependence on the incident kinetic energy, showing a modest (statistically significant) increase initially (from $E_i=5.1$ to 7.7 eV), and a slight (statistically insignifi-

cant) decrease as E_i is increased from 7.7 to 12.3 eV. At thermal energies (~ 0.1 eV) we expect $S=1$, and likely independent of coverage. Thus, if the values at $E_i=5.1$ eV are quantitatively correct, this would imply that the adsorption probability at high coverage passes through a minimum—behavior that is reminiscent of the adsorption probability of a transition metal complex on a surface terminated with a self-assembled monolayer.[36] Nevertheless, for five of the eight conditions/substrates examined the normalized probabilities in the high coverage regime are between 0.9 and 1, within the estimated experimental uncertainty. This suggests that, over the incident kinetic energy regime considered here, the adsorption and accommodation of the molecule's incident kinetic energy are efficient.

In contrast with the results at high coverage, on both substrates the implied probabilities of adsorption at zero coverage, S_0, are much less than unity, and show a clear trend with increasing incident kinetic energy, decreasing with increasing E_i. While the adsorption probabilities at high coverage for a particular value of E_i are very similar on the two substrates, and within 10% of each other for all cases, this is not the case for the zero-coverage probability of adsorption, which exhibits a dependence on the substrate. For all values of E_i, the probability of adsorption is smaller on the HMDS-modified surface.

We can make an additional comparison by calculating the ratio of S_0 to $S_{n\geq 1}$. For example, should the modest increase in $S_{n\geq 1}$ as E_i is increased from 5.1 to 7.7 eV we observe here not be physical, but perhaps some artifact in our estimation of the incident flux, then this procedure might be a better estimate for S_0, assuming that $S_{n\geq 1}\sim 1$. These results are shown in Fig. 6 for both surfaces, where the dashed line acts to guide the eye. As may be seen, in both cases there is smooth decrease in the ratio $S_0/S_{n\geq 1}$ with increasing energy on both surfaces.

Given knowledge of the adsorption probability of DIP on these two substrates it is of interest to compare these to the values that we measure for pentacene on these same two surfaces.[18,19] DIP and pentacene are of course similar organic molecules, both planar, with a rather large length-to-width aspect ratio. Thus we may expect similar behavior concerning the dynamics of trapping. Ignoring for the moment the angle of incidence, as all of the results here are for normal incidence, in most simple models for trapping the incident kinetic energy (E_i), the binding energy of the molecule to the surface (E_{ads}), the mass of the incident particle, and the (effective) mass of the surface atom(s) play roles in determining the adsorption probability. One can expect that the trapping probability should be a smoothly decreasing function of a reduced kinetic energy, E_i/E_{ads}. As DIP and pentacene are expected to bind flat to the surface at low coverage (we assume accommodation occurs before subsequent transport and incorporation into existing islands), and since they are planar, one might expect that the binding energy E_{ads} will scale approximately with the number of C atoms.

In Figs. 7 and 8 we display the adsorption probability measured for DIP and pentacene[18,19] on SiO_2 and HMDS-modified SiO_2 plotted as a function of the reduced incident kinetic energy. In both cases the values for the adsorption
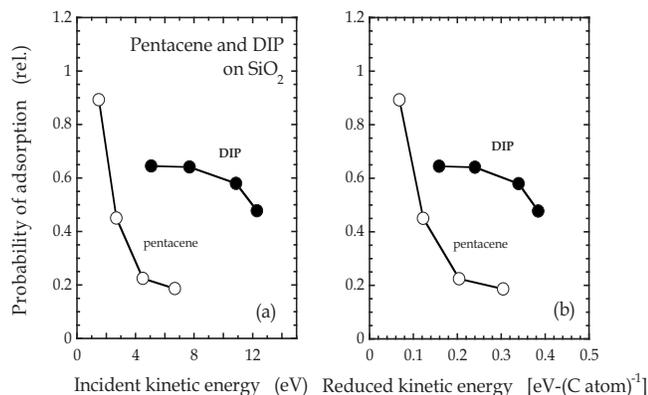
FIG. 7. Relative (initial) probabilities of adsorption of DIP and pentacene on SiO$_2$ plotted vs (a) incident kinetic energy and (b) a reduced kinetic energy. The reduced kinetic energy represents simply the incident kinetic energy per C atom. All data have been normalized to the highest GR observed in each case (see text).

probabilities were normalized to the highest GR (also flux normalized) observed in the multilayer regime, which for pentacene was found at $E_i = 1.5$ eV, and for DIP at $E_i = 7.7$ eV. To arrive at a reduced kinetic energy we simply divide E_i by the number of C atoms in each molecule.

In Fig. 7(a) we see that there is a significant difference between the adsorption probabilities for DIP and pentacene on SiO$_2$ at a similar value of E_i. The difference is less when the data are plotted as a function of the reduced kinetic energy in Fig. 7(b), however, the data still do not exhibit much similarity. This is surprising, and we do not have a good explanation for this. We note that these two data sets (DIP and pentacene) were collected using different experimental systems and techniques (x-ray scattering versus AFM). It is possible that these experiments were conducted under different partial pressures of H$_2$O. However, both systems possess a base pressure of no greater than 5×10^{-9} Torr, and both systems use a load lock for sample entry, thus differences in the presence of H$_2$O(a) would not seem to be the basis for an explanation. Additional experiments may be warranted.

In Fig. 8 we consider the results for DIP and pentacene on HMDS-modified SiO$_2$. As may be seen, plotted versus the
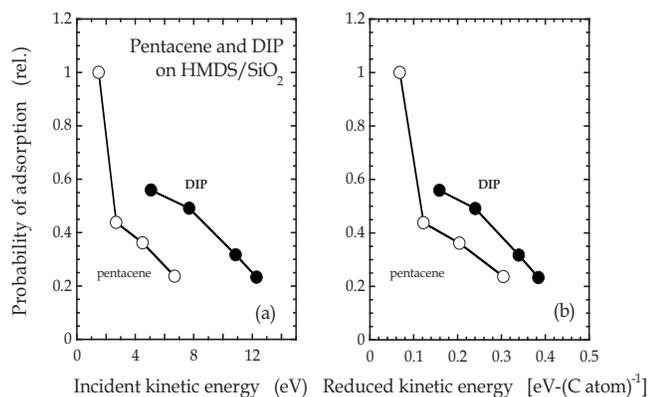
FIG. 8. Relative (initial) probabilities of adsorption of DIP and pentacene on SiO$_2$ modified with HMDS plotted vs (a) incident kinetic energy and (b) a reduced kinetic energy. The reduced kinetic energy represents simply the incident kinetic energy per C atom. All data have been normalized to the highest GR observed in each case (see text).

reduced kinetic energy the two sets of data now exhibit similar behavior. The probability of adsorption of DIP exceeds that for pentacene by a modest amount at a comparable value of E_i/E_{ads}, however, the construction has not produced a universal curve. A number of factors might contribute to the fact that a universal curve is not observed. For example, we have not considered excitation of internal modes in the two molecules. Such $T \rightarrow V$ conversion, if more prevalent for the larger DIP molecule, it would imply that internal energy might also play a role in determining the adsorption probability (e.g., vibrationally hot molecules will trap less efficiently). In previous work on NO trapping on Au(111) (Ref. 37) vibrational energy had no effect on trapping. Concerning the trapping of more complex molecules (SF$_6$ and CCl$_4$) on their condensed phases[38] an effect of vibrational energy was observed, but it vanished at higher incident kinetic energies. Thus, the role of internal energy remains to be determined.

In concluding our discussion of the dynamics of adsorption we now make a number of conclusions and observations. First, there is clearly a difference between the dynamics of trapping on the bare surfaces and the growing thin film of DIP. This is the major result of this work. This result mostly reflects very efficient trapping on the surface covered by DIP due to highly efficient momentum transfer due to mass matching. In general the well depths of the molecule-surface potentials for DIP on SiO$_2$, HMDS-modified SiO$_2$ and a DIP thin film are unknown. The latter is most easily related to the enthalpy of sublimation, which for pentacene is about 1.6 eV.[39] Given a well depth of this order, it is somewhat surprising that at $E_i = 12.3$ eV that trapping of DIP on DIP is as efficient as it apparently is. One factor that assists trapping in this high kinetic energy regime is likely direct molecular insertion, which we will discuss further below. Trapping on the bare surface exhibits behavior similar to that observed in many small-molecule-surface systems—it exhibits a continuous decrease with increasing kinetic energy. For DIP, trapping is more efficient on the untreated SiO$_2$ surface. As stated above the molecule-surface potential is generally not known for the two systems considered here. Comparing the two surfaces it would seem that excitation of surface vibrational modes/phonons may not be so different, as the –OH present on SiO$_2$ is basically replaced by a –O–Si(CH$_3$)$_3$ species. Finally, electron excitation seems unlikely as SiO$_2$ is a large band gap insulator.

In addition to analysis of the rate of adsorption as a function of coverage we have also examined the morphological evolution of the thin films also as a function of coverage. Although this topic is not the focus of this paper, it is instructive to comment on those features that might shed some light as to the molecular scale events occurring during adsorption. The evolution of surface roughness can be assessed by the modeling of the anti-Bragg oscillations we considered above (Figs. 2–5) and by direct measurement using AFM. In Fig. 9 we present the rms surface roughness predicted by our fits to the anti-Bragg oscillations as a function of film thickness for growth of DIP on (a) SiO$_2$ and (b) HMDS-modified SiO$_2$. Also shown as individual points, are the rms surface roughness values found from analysis of the AFM images (in each case, 3×3 μm^2 and 10×10 μm^2). First, on HMDS-
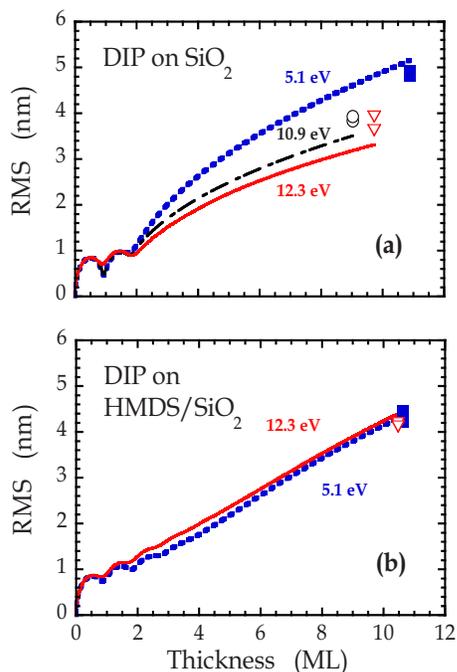
FIG. 9. (Color online) Thin film roughness as a function of thin film thickness for DIP deposited on (a) clean SiO_2 and (b) SiO_2 modified with HMDS. Results are shown for 3 and 2 values of the incident kinetic energy, respectively. The curves represent the prediction of the model used to fit the anti-Bragg intensity data shown in Figs. 2–5. The points shown represent roughness values obtained directly from AFM. $E_i=5.1$ eV (short dash, filled squares); 10.9 eV (short/long dash, circles); 12.3 eV (solid line, triangles).

modified SiO_2 we see in (b) that there is very little difference in the evolution of surface roughness. The two data sets not plotted ($E_i=7.7$ and 10.9 eV) are essentially indistinguishable from the two that are plotted ($E_i=5.1$ and 12.3 eV). Concerning the final rms roughness, for all four values of E_i examined, the standard deviations between the value predicted from the x-ray analysis, and those measured from AFM do not exceed 4%.

As may be seen in Fig. 9(a), on SiO_2, in contrast, we do observe an identifiable trend with kinetic energy, and the increase in roughness is slowest at the highest kinetic energy. Note that the intermediate energy (7.7 eV, not plotted) exhibits results almost indistinguishable from those shown for the lowest kinetic energy (5.1 eV). In all of these cases, the discrepancy between the predictions of the model and the results from AFM span the range 3%–8%. The roughness found from AFM also decreases continuously with increasing kinetic energy, in agreement with the predictions of the model fit to the x-ray data.

What factors might lead to a decrease in surface roughness with increasing incident kinetic energy? First we recall that flux normalized GRs/relative adsorption probabilities at high coverage do not vary substantially with kinetic energy, and are very similar on the two surfaces examined. Thus, changes in the morphological evolution due to different GRs can be ruled out. Other factors/explanations often associated with thin film growth using energetic particles are the formation of "hot spots," and so-called transient mobility where molecules can skitter across the surface before being fully thermalized and finding a favorable binding site. In prelimi-

nary work, we have found that smoother films can be formed by increasing the substrate temperature (both on SiO_2 and HMDS-modified SiO_2). What is curious, however is how such hot spots could be produced and modify the growth on SiO_2, but not on HMDS-modified SiO_2? If transient mobility is a major factor, again why would it be present for growth on SiO_2, and not on HMDS-modified SiO_2?

From experiment, there are no obvious clues as to what may be changing as to the ultimate destination of molecules impacting the growing crystal. Some insight can be obtained from molecular simulation, where the adsorption of pentacene on a pentacene crystal has been investigated. Briefly, from these studies,[28,29] it is found that there is an increasing tendency for molecules striking first the nth layer to become part of *that* layer, and *not* the nth+1 layer, via direct molecular insertion or, if the impact is sufficiently close to a step edge, via transport across the step edge. For example, at $E_i=2$ eV and for impacts 11 Å from the step edge nearly $\frac{3}{4}$ of the molecules simply adsorb on top of the existing layer, while $\sim 20\%$ directly incorporate into that layer. As E_i is increased further to 5 and then 10 eV these numbers change dramatically, with the fraction residing on top decreasing to about $\frac{1}{2}$ and then 20%, while the fraction directly incorporating into the preexisting layer increasing to 28% and then 40%. Thus, it would seem that events such as direct molecular insertion may play a role here. For an incompletely filled and exposed layer, molecular insertion would seem to be beneficial to smooth growth, as it will promote completion of the nth layer before growth of the nth+1 layer has become significant. Direct molecular insertion could also be detrimental to smooth growth, however, as it can produce interstitial species directly, which can cause the buildup of stress in the film that might lead to deleterious strain-relief mechanisms causing roughening. If energy dependent direct molecular insertion is playing a role in determining the thin film morphological evolution, then why would it be most evident on SiO_2? As discussed below, the biggest difference between the two surfaces occurs at $E_i=5.1$ eV and as the coverage increases from 2 to 4 ML. It is conceivable that in this coverage regime the island density and shape may depend on substrate surface termination in such a way that it affects the amount of direct insertion or related processes such as "downward funneling."[40]

One final factor may play a role in the structural evolution—it is well known, for example, that organic thin films can often crystallize in different phases, often as a function of thin film thickness. For what film thicknesses may this issue be important here? Side-by-side comparison of the roughness versus thickness shows that the difference between the two surfaces is largest at the lowest incident kinetic energy, $E_i=5.1$ eV. Moreover, the majority of the difference is associated with the morphological evolution from 2 to 4 ML: for $E_i=5.1$ eV on SiO_2 the roughness is 1.12 to 2.63 nm over this range, a change of 1.51 nm, while on HMDS-modified SiO_2 it is 1.11–1.77 nm, a change of 0.66 nm. In comparison, for $E_i=5.1$ eV at a coverage of 10 ML on SiO_2 the roughness is 4.14 nm, a change (from the value at 4 ML) of 2.37 nm, whereas on HMDS-modified SiO_2 the roughness is 4.90 nm, a change of 2.27 nm. Previ-

ous work[35] may be of interest here to the discussion, where the growth of DIP on SiO_2 was examined at thermal kinetic energies and $T_s = 130\ °C$. Here on SiO_2 a change in the in-plane lattice parameter, a 2% expansion, was observed upon the adsorption of the second and third MLs. In work not to be detailed here, we observe a similar expansion in the in-plane parameter for this same coverage regime for DIP on HMDS-modified SiO_2 at $E_i = 10.8$ eV. Thus, these structural changes, seen on both surfaces, would seem to not explain the differences in the dependence of roughening on kinetic energy observed here between DIP grown on SiO_2 and that grown on HMDS-modified SiO_2.

IV. CONCLUSIONS

We have examined the dynamics of adsorption of DIP on SiO_2 and SiO_2 modified with an interfacial organic layer using *in situ* real time synchrotron x-ray scattering, focusing on the effects of coverage. On both surfaces we observe a substantial difference between the dynamics of adsorption on the clean surfaces, and that on the growing thin film. On the clean surfaces, we observe a smooth decrease in the probability of adsorption with increasing incident kinetic energy, which is reminiscent of trapping-mediated adsorption seen in many systems. For DIP, trapping is somewhat more efficient on the clean SiO_2 surface, perhaps due to a larger binding energy of DIP to this surface. Once both surfaces are covered by DIP, the effects of incident kinetic energy are greatly reduced, and trapping is very efficient over the range of kinetic energies examined. Possible reasons for efficient trapping at high coverage and at high incident kinetic energy (E_i exceeding the binding energy by a factor of 5–10) include more efficient momentum transfer due to mass matching, and possibly direct molecular insertion. These differences between the dynamics of adsorption in the submonolayer and multilayer regimes lead to significant accelerations in the rate of growth, approaching a factor of 4 in one case. Finally, the evolution of surface roughness is similar for all incident kinetic energies and, on both surfaces, layer-by-layer growth is severely degraded after deposition of 4 ML. We do observe a modest effect of kinetic energy on roughening for growth of DIP on SiO_2, where the degradation of layer-by-layer growth is most rapid for deposition at the lowest incident kinetic energy examined ($E_i = 5.1$ eV).

[1] Y. Y. Lin, D. J. Gundlach, S. F. Nelson, and T. N. Jackson, IEEE Electron Device Lett. **18**, 606 (1997).
[2] T. W. Kelley, L. D. Boardman, T. D. Dunbar, D. V. Muyres, M. J. Pellerite, and T. P. Smith, J. Phys. Chem. B **107**, 5877 (2003).
[3] S. Verlaak, S. Steudel, P. Heremans, D. Janssen, and M. S. Deleuze, Phys. Rev. B **68**, 195409 (2003); S. Verlaak, V. Arkhipov, and P. Heremans, Appl. Phys. Lett. **82**, 745 (2003).
[4] R. Ruiz, D. Choudhary, B. Nickel, T. Toccoli, K.-C. Chang, A. C. Mayer, P. Clancy, J. M. Blakely, R. L. Headrick, S. Iannotta, and G. G. Malliaras, Chem. Mater. **16**, 4497 (2004).
[5] C. D. Dimitrakopoulos, A. R. Brown, and A. Pomp, J. Appl. Phys. **80**, 2501 (1996).
[6] J. G. Laquindanum, H. E. Katz, A. J. Lovinger, and A. Dodabalapur, Chem. Mater. **8**, 2542 (1996).
[7] D. Knipp, R. A. Street, A. Volkel, and J. Ho, J. Appl. Phys. **93**, 347 (2003).
[8] R. Ruiz, B. Nickel, N. Koch, L. C. Feldman, R. F. Haglund, Jr., A. Kahn, F. Family, and G. Scoles, Phys. Rev. Lett. **91**, 136102 (2003).
[9] A. C. Mayer, R. Ruiz, R. L. Headrick, A. Kazimirov, and G. G. Malliaras, Org. Electron. **5**, 257 (2004).
[10] T. W. Kelley, L. D. Boardman, T. D. Dunbar, D. V. Muyres, M. J. Pellerite, and T. P. Smith, J. Phys. Chem. B **107**, 5877 (2003).
[11] H. Yang, T. J. Shin, M.-M. Ling, K. Cho, C. Y. Ryu, and Z. Bao, J. Am. Chem. Soc. **127**, 11542 (2005).
[12] V. Ignatescu, J.-C. M. Hsu, A. C. Mayer, J. M. Blakely, and G. G. Malliaras, Appl. Phys. Lett. **89**, 253116 (2006).
[13] P. Milani and S. Iannotta, *Cluster Beam Synthesis of Nanostructured Materials* (Springer-Verlag, Berlin, 1999).
[14] A. J. Salih, S. P. Lau, J. M. Marshall, J. M. Maud, W. R. Bowen, N. Hilal, R. W. Lovitt, and P. M. Williams, Appl. Phys. Lett. **69**, 2231 (1996).
[15] M. Shtein, P. Peumans, J. B. Benziger, and S. R. Forrest, J. Appl. Phys. **96**, 4500 (2004).
[16] L. Casalis, M. F. Danisman, B. Nickel, G. Bracco, T. Toccoli, S. Iannotta, and G. Scoles, Phys. Rev. Lett. **90**, 206101 (2003).
[17] S. Iannotta and T. Toccoli, J. Polym. Sci., Part B: Polym. Lett. **41**, 2501 (2003).
[18] A. S. Killampalli, T. W. Schroeder, and J. R. Engstrom, Appl. Phys. Lett. **87**, 033110 (2005).
[19] A. S. Killampalli and J. R. Engstrom, Appl. Phys. Lett. **88**, 143125 (2006).
[20] T. Toccoli, A. Pallaoro, N. Coppede, S. Iannotta, F. De Angelis, L. Mariucci, and G. Fortunato, Appl. Phys. Lett. **88**, 132106 (2006).
[21] Y. Wu, T. Toccoli, N. Koch, E. Iacob, A. Pallaoro, P. Rudolf, and S. Iannotta, Phys. Rev. Lett. **98**, 076601 (2007).
[22] S. Hong, A. Amassian, A. R. Woll, S. Bhargava, J. D. Ferguson, G. G. Malliaras, J. D. Brock, and J. R. Engstrom, Appl. Phys. Lett. **92**, 253304 (2008).
[23] O. F. Hagena and W. Obert, J. Chem. Phys. **56**, 1793 (1972).
[24] H. T. Jonkman, U. Even, and J. Kommandeur, J. Phys. Chem. **89**, 4240 (1985).
[25] See, e.g., C. T. Rettner, D. J. Auerbach, J. C. Tully, and A. W. Kleyn, J. Phys. Chem. **100**, 13021 (1996).
[26] G. M. Nathanson, Annu. Rev. Phys. Chem. **55**, 231 (2004).
[27] S. R. Cohen, R. Naaman, and J. Sagiv, Phys. Rev. Lett. **58**, 1208 (1987); F. Schreiber, Prog. Surf. Sci. **65**, 151 (2000).
[28] J. E. Goose and P. Clancy, J. Phys. Chem. C **111**, 15653 (2007).
[29] J. E. Goose, A. Killampalli, P. Clancy, and J. R. Engstrom, "Molecular-scale events in hyperthermal deposition of organic semiconductors implicated from experiment and molecular simulation," J. Phys. Chem. C (in press).
[30] A. C. Dürr, F. Schreiber, M. Münch, N. Karl, B. Krause, V. Kruppa, and H. Dosch, Appl. Phys. Lett. **81**, 2276 (2002).
[31] T. W. Schroeder, Ph.D. thesis, Cornell University, 2004.
[32] A. R. Woll, T. V. Desai, A. Amassian, S. Hong, and J. R. Engstrom (unpublished).
[33] P. I. Cohen, G. S. Petrich, P. R. Pukite, G. J. Whaley, and A. S. Arrott, Surf. Sci. **216**, 222 (1989).
[34] B. Krause, F. Schreiber, H. Dosch, A. Pimpinelli, and O. H. Seeck, Europhys. Lett. **65**, 372 (2004).
[35] S. Kowarik, A. Gerlach, S. Sellner, F. Schreiber, L. Cavalcanti, and O. Konovalov, Phys. Rev. Lett. **96**, 125504 (2006).

[36] P. F. Ma, A. Dube, A. S. Killampalli, and J. R. Engstrom, J. Chem. Phys. **125**, 034706 (2006).

[37] A. M. Wodtke, H. Yuhui, and D. J. Auerbach, Chem. Phys. Lett. **413**, 326 (2005).

[38] S. J. Sibener and Y. T. Lee, J. Chem. Phys. **101**, 1693 (1994).

[39] V. Oja and E. M. Suuberg, J. Chem. Eng. Data **43**, 486 (1998).

[40] K. J. Caspersen, C. R. Stoldt, A. R. Layson, M. C. Bartelt, P. A. Thiel, and J. W. Evans, Phys. Rev. B **63**, 085401 (2001).